Dynamics of Surf-Zone Turbulence in a Strong Plunging Breaker

by

Francis C. K. Ting and James T. Kirby

Research sponsored by
Office of Naval Research
Grant N00014-90-J168

RESEARCH REPORT NO. CACR-94-21
November, 1994

Center for Applied Coastal Research
Ocean Engineering Laboratory
University of Delaware
Newark, DE 19716

Dynamics of surf-zone turbulence in a strong plunging breaker

Francis C. K. Ting [1], **James T. Kirby** [2]

[1] *Ocean Engineering Program, Department of Civil Engineering, Texas A&M University, College Station, TX 77843*

[2] *Center for Applied Coastal Research, Department of Civil Engineering, University of Delaware, Newark, DE 19716*

Abstract

The characteristics of turbulence created by a strong plunging breaker on a 1 on 35 plane slope have been studied experimentally in a two-dimensional wave tank. The experiments involved detailed measurements of fluid velocities below trough level and water surface elevations in the surf zone using a fiber-optic laser-Doppler anemometer and a capacitance wave gage. The dynamical role of turbulence is examined making use of the transport equation for turbulent kinetic energy (the k-equation). The results show that turbulence under a plunging breaker is dominated by large-scale motions and has certain unique features that are associated with its wave condition. It was found that the nature of turbulence transport in the inner surf zone depends on a particular wave condition and it is not similar for different types of breakers. Turbulent kinetic energy is transported landward under a plunging breaker and dissipated within one wave cycle. This is different from spilling breakers where turbulent kinetic energy is transported seaward and the dissipation rate is much slower. The analysis of the k-equation shows that advective and diffusive transport of turbulence play a major role in the distribution of turbulence under a plunging breaker, while production and dissipation are not in local equilibrium but are of the same order of magnitude. Based on certain approximate analytical approaches and experimental measurements it is shown that turbulence produc-

tion and viscous dissipation below trough level amount to only a small portion of the wave energy loss caused by wave breaking. It is suggested that the onshore sediment transport produced by swell waves may be tied in a direct way to the unique characteristics of turbulent flows in these waves.

---

1. Introduction

Plunging breakers have aroused great interest among coastal engineers for many years. The classical form is characterized by the formation of an overturning jet, in which the front face of the wave becomes vertical and the crest curls over and plunges into the water ahead with considerable force. Plunging breakers play an important role in dynamic equilibrium of beaches. It is well known that waves that develop into plunging breakers tend to build up beaches. In most situations, the milder and longer period swell waves following a storm would transport sand from the offshore bars to be re-deposited on the foreshore, and in this way the beach begins to recover from the storm attack. The physical mechanisms that allow swell waves to move sediment onshore may also be used to advantage in shoreline protection. For instance, the U.S. Army Corps of Engineers has recently investigated the use of suitable dredged material to construct feeder berms in the nearshore zone (McLellan 1990, McLellan and Kraus 1991). Such berms are expected to behave similarly to natural bars in their interaction with waves, and provide a sand source for the beach profile during periods of accretionary wave conditions. The study of plunging breakers clearly has important engineering applications. Nevertheless, we still have only a vague understanding of the fundamental nature of these waves.

Several investigators have studied plunging breakers under controlled laboratory conditions. A qualitative description of the features of plunging breakers in

the outer region of the surf zone can be found in Peregrine (1983), Basco (1985) and Battjes (1988), among others. Wave breaking is characterized by a sudden, violent transition from irrotational to rotational motion, then several cycles of splash-up and plunge which transform the large-scale, vortex motions into a turbulent bore. Basco (1985) hypothesized that the water body pushed up by the overturning jet creates a secondary wave with new wave kinematics in the surf zone. These observations suggest that the process of transformation from organized wave motion into turbulent motion in a plunging breaker is fundamentally different from other types of breakers. Hence, it is natural to expect that the turbulent flow created by a plunging breaker might have certain unique characteristics that are associated with its wave condition.

With the advent of laser-Doppler anemometry several investigators have measured the velocity fields under plunging breakers. Some of the more detailed studies include Stive (1980), Nakagawa (1983), Hattori and Aono (1985), Mizuguchi (1986), and Okayasu et al. (1986). Stive (1980) measured two velocity components and dynamic pressure under spilling and plunging breakers on a 1 on 40 slope. He concluded that the flow fields in the inner surf zone are similar for different deep-water wave conditions. He also found that the pressure distribution deviates from hydrostatic pressure under the breaking wave front and the wave crest due to effects of vertical velocity.

Nakagawa (1983) measured three velocity components of water particles in a two-dimensional wave flume using a tension-thread velocity meter. He concluded that the transverse velocities are comparable to the vertical and horizontal velocities. Hattori and Aono (1985) studied turbulence structures under spilling and plunging breakers where two velocity components were measured using a split-type hot film anemometer. The turbulent component of the velocity signal was

extracted using Fourier analysis assuming that (1) the wave-induced velocity is linearly related to the water surface elevation, and (2) the turbulent velocity and the water surface elevation are not correlated. In both afore-mentioned studies wave breaking was initiated at the edge of a horizontal shelf by a 1 on 20 slope in front. In this way the position where the wave breaks is controlled; however, this may impose an unnatural condition on the breaking process itself.

Mizuguchi (1986) measured the spatial and temporal distributions of horizontal and vertical velocity components in the outer region of a laboratory surf zone using a laser-Doppler anemometer. Wave breaking was created by a plunging breaker on a 1 on 20 plane slope. The flow fields obtained from this study represent some of the most detailed experimental measurements of this kind. The organized wave-induced motion was obtained by phase-averaging the velocity signal over forty successive waves, while the deviations from the phase average were considered to be the turbulent fluctuations. Additionally, the water particle acceleration and the vorticity fields were obtained from the measured velocity fields. Similar experiments were conducted by Okayasu et al. (1986) for numerous locations inside the surf zone. They also obtained the time-mean eddy viscosity from the time-mean Reynolds stress and the vertical gradient of the undertow. They found that the mean Reynolds stress and the mean eddy viscosity decreased with distance from the surface.

Previous studies of breaking waves have greatly improved our knowledge of the surf zone, but the present state of the art is still far from satisfactory. There have been very little applications of theory of turbulence in this field of research. Consequently, many basic features of the turbulent flows and their effect on surf-zone dynamics are understood only qualitatively. For example, turbulence

transport has not been studied in a systematic manner for different types of breakers. In the case of sediment transport modeling, it is essential to predict the spatial and temporal variations of turbulent kinetic energy in order to model the rates and direction of sediment transport. The distribution of turbulent kinetic energy is described by the energy equation for the turbulence (the k-equation). For high Reynolds numbers, the k-equation shows that the local time rate of change of turbulent kinetic energy is due to convection by the mean flow, diffusive transport by velocity and pressure fluctuations, turbulent energy production, and viscous dissipation. The relative importance of these terms are important in turbulence modeling and must be determined, for some problems do not warrant the complexity of solving the full k-equation. Previously, Deigaard et al. (1986) have modeled the distribution of turbulence under spilling and plunging breakers using the k-equation. They neglected the horizontal advection and diffusion terms under the assumption that horizontal gradients are small compared to vertical gradients. This approach may be reasonable for spilling breakers. In a plunging breaker the temporal variations of turbulence intensities over a wave period are much higher and there is a strong upward flow underneath the wave front. Hence, in addition to diffusion of turbulence, convection of turbulence by organized wave-induced flow plays a major part. In this present study, dynamics of turbulence in a strong plunging breaker is studied through an experimental investigation of the transport equation for turbulent kinetic energy. First, we present measurements of turbulent kinetic energy and energy flux in a laboratory surf zone, and discuss how the mean flow and the velocity fluctuations move turbulent energy under a plunging breaker. We find that advection plays an important role in the transport of turbulence. It turns out that turbulent kinetic energy is carried upward and landward by the mean flow

under the plunging breaker. If it is assumed that turbulent fluctuations are responsible for keeping sediment in suspension, and the transport of sediment is given by the convection of the fluid-grain mass, then suspended sediment transport superficially resembles turbulence transport by mean flow, and there would be a generally shoreward directed suspended sediment transport under the plunging breaker. We then examine the relative importance of the terms in the k-equation. In order to gain an appreciation of the dynamical role of turbulence, it is useful to discuss a number of questions, such as (1) How is the kinetic energy of the turbulence maintained ? (2) How much turbulent energy is generated below trough level ? (3) How does turbulent energy spread downward ? (4) How fast does turbulent energy spread downward relative to its dissipation rate and how much energy is dissipated below trough level ? (5) How does turbulence transport differ between spilling and plunging breakers? The analysis of these problems give us a picture of the dynamical role of turbulence in these waves. This work is the first step in the long process of developing turbulence models for the surf zone.

2. Experimental equipment and procedure

The measurements from which the present results were derived are partly used in a previous study (Ting and Kirby, 1994). To prevent duplication of the description of details just a brief account of the experimental equipment and procedure is given below.

The experiments were conducted in a two-dimensional wave tank located in the Ocean Engineering Laboratory at University of Delaware. The wave tank was 40 m long, 0.6 m wide and 1.0 m deep. The tank was equipped with a bulkhead wave generator, which accepted an input voltage from an IBM PS/2

Model 30 286 computer. A plywood false bottom was installed in this wave tank to create a uniform slope of 1 on 35. The slope was sealed to the tank walls by inserting a polystyrene rod in between the edges of the slope and the side walls, and then filling the gap with silicone.

A schematic diagram of the experimental arrangement and the coordinate system is shown in Fig. 1. We shall use the following notations in this paper; ζ is the instantaneous water surface elevation, $\overline{\zeta}$ is the mean water surface elevation, d is the local still water depth, $h = d + \overline{\zeta}$ is the local mean water depth, and the subscript b denotes the wave breaking point. The still water depth in the constant-depth region was 0.4 m. The waves used in this study were cnoidal waves. The wave height in the constant-depth region was 12.8 cm, and the wave period was 5.0 s. The ratio of deep-water wave height H_0 to deep-water wavelength L_0 was 0.0023 based on linear shoaling. These conditions produced a strong plunging breaker of height 19.1 cm at the breaking point ($x_b = 7.795$ m, $d_b = 15.6$ cm). Breaking point of the plunging breaker is defined as the location where front face of the wave becomes nearly vertical.

Water surface elevations and velocities were measured at seven locations along the centerline of the wave tank; their exact locations are given in Table 1. The horizontal distance covered by the measuring section was 3.1 m, extending from $d = 16.9$ cm just before wave breaking to $d = 7.9$ cm in the inner surf zone. It was observed that H/h approached a limiting value of 0.8 at $x = 10.395$ m. Hence, this station may be considered to be the beginning of the inner surf zone. Water surface elevation was measured using a capacitance wave gage. Water particle velocities were obtained using a two-component fiber-optic laser-Doppler anemometer (LDA) built by Dantec Electronics. The LDA was a backscatter, four-beam laser system. It consisted of a 100 mW air-cooled argon-ion laser,

a transmitter, a 14 mm probe (focal length 50 mm, beam spacing 8 mm) and one frequency tracker and shifter for each velocity component. However, only the green line (wavelength 514.5 nm) of the argon-ion laser was used because the laser did not have enough power to operate the blue beams (wavelength 488 nm). Thus, horizontal and vertical velocities were obtained by conducting the same experiment twice. The frequency trackers recorded a velocity offset when tested in still water conditions. The estimated inaccuracies of the LDA due to this velocity offset amount to ± 0.5 cm/s. The wave gage and the fiber-optic probe were mounted on an instrument carriage which could slide along the top of the tank on two rails. The probe was submerged in water during experiment, and the mounting mechanism of the LDA was such that any desired vertical location in the flume could be reached.

Periodic waves were generated for a minimum of 20 minutes before data were taken. Hence, the measured flow corresponded to a steady-state condition in the wave tank. Data were taken by an IBM PS/2 Model 30 286 computer equipped with a MetraByte DASH-16(F) data acquisition board. Measurements consisted of time histories of wave plate motion, water surface elevation, Doppler and lock detector signals. One hundred and two successive waves were recorded with a sampling frequency of 100 Hz for each channel. The wave plate motion was used later to synchronize the velocity time histories from different probe locations.

The water was seeded with titanium oxide particles to scatter the laser light. The use of scattering particles greatly improved the quality of Doppler signals and minimized signal drop-out. During experiment, entrained air in the flow sometimes blocked the laser beams resulting in signal drop-out. When signal drop-out occurred the tracker was not locked to the frequency of the Doppler signal and the Doppler frequency was held at the last measured value.

These events were detected by a built-in lock detector whose logic state would change from HIGH to LOW during signal drop-out. In order to reduce the influence of aeration on the velocity measurements, velocity signals that were associated with a LOW state were not used in data analysis. Because of this, the number of velocity measurements that were actually used in computing a phase average were less than one hundred and two. The percentage of signal drop-out depended on seeding condition and measuring location; it was between 5% and 40% at the trough level inside the surf zone. However, we have sampled such a large number of waves that there were always enough realizations to achieve stable wave and turbulence statistics (see, Ting and Kirby 1994). The organized wave-induced flow was found as the phase average of the instantaneous velocity field, while deviations from the phase average were considered to be turbulent velocity fluctuations. For a detailed description of the experimental procedure the interested reader is referred to Ting and Kirby (1994).

3. Turbulence transport equation

In the analysis of fluid-sediment interaction the turbulent kinetic energy is important in determining the turbulent mixing coefficient and thus the turbulent mass transport. The turbulent mixing coefficient may be written as the product of a length scale and a velocity scale. A physical meaningful velocity scale is $\sqrt{k}$, where k is the turbulent kinetic energy. Therefore, the determination of the temporal and spatial variations of turbulent kinetic energy is of utmost importance in the calculation of sediment transport. The distributions of k may be determined by solving the the energy equation for the turbulence. For high Reynolds numbers (this will be discussed), the k-equation reads (see, Tennekes

and Lumley 1972)

$$\frac{\partial k}{\partial t} + \frac{\partial \tilde{u}_j k}{\partial x_j} = -\frac{\partial}{\partial x_j}\left(\frac{1}{\rho}\widetilde{u_j' p'} + \widetilde{u_j' k'}\right) - \widetilde{u_i' u_j'} S_{ij} - 2\nu \widetilde{s_{ij} s_{ij}} \tag{1}$$

where

$$k = \frac{1}{2}\widetilde{u_i' u_i'}, \qquad k' = \frac{1}{2} u_i' u_i', \tag{2}$$

S_{ij} is the mean rate of strain, defined by

$$S_{ij} = \frac{1}{2}\left(\frac{\partial \tilde{u}_i}{\partial x_j} + \frac{\partial \tilde{u}_j}{\partial x_i}\right), \tag{3}$$

and s_{ij} is the fluctuating rate of strain, defined by

$$s_{ij} = \frac{1}{2}\left(\frac{\partial u_i'}{\partial x_j} + \frac{\partial u_j'}{\partial x_i}\right). \tag{4}$$

In Eq. 1, the tilde is an operator is to take a phase average, t is time, x_j ($j = 1,2,3$; $x_1 = x$, $x_2 = y$, $x_3 = z$) are the coordinates of a Cartesian frame with z extending positive upward from the still water level, $\tilde{u}_j$ ($j = 1,2,3$; $\tilde{u}_1 = \tilde{u}$, $\tilde{u}_2 = \tilde{v}$, $\tilde{u}_3 = \tilde{w}$) are the components of phase-averaged velocity, u_j' and p' are the fluctuating parts of velocity and pressure, ρ is density, and ν is kinematic viscosity. In the Reynolds averaging process, the instantaneous water particle velocities u_j are separated into the sum of an organized and a turbulent contribution, i.e., $u_j = \tilde{u}_j + u_j'$. The organized wave-induced flow (mean flow), $\tilde{u}_j$, includes both the orbital wave motion and the undertow.

Equation (1) shows that the local time rate of change of turbulent kinetic energy is due to convection by mean flow, diffusive transport by pressure and turbulent fluctuations, turbulent energy production, and viscous dissipation. Much insight about surf-zone dynamics can be gained from a detailed analysis of Eq. 1. At the present time, it is believed that the main part of production of turbulent kinetic energy takes place in the surface roller, spreading of turbulent

energy is primarily due to convection (Svendsen, 1987). It is also thought that the rate of dissipation of turbulent energy is high in the surface roller, whereas only a small portion of the energy loss in the breaking wave is dissipated below trough level. These statements require experimental confirmation. The convective transport and the production terms may be found from the instantaneous velocity measurements, and we will study them. On the other hand, it is more difficult to obtain the diffusive transport terms. Because of this, in turbulence modeling turbulent diffusion is often assumed proportional to the gradient of k (Rodi, 1984), i.e.

$$-\left(\widetilde{u_j' k'} + \widetilde{u_j' \frac{p}{\rho}}\right) = \frac{\nu_t}{\sigma_k} \frac{\partial k}{\partial x_j} \tag{5}$$

where ν_t is the eddy viscosity and σ_k is an empirical diffusion constant. It can be seen that measurements of the terms of diffusion require three velocity components of water particle as well as the dynamic pressure of turbulence. The pressure-velocity correlation terms are especially important. They exchange energy between components of turbulent fluctuations, and contribute significantly to the diffusion of turbulent kinetic energy. Since we did not measure the Reynolds stresses and the dynamic pressure, the present study is somewhat inconclusive in determining the nature of turbulent diffusion.

The viscous dissipation term $2\nu \widetilde{s_{ij} s_{ij}}$ is determined from velocity measurements making use of the theory of isotropic turbulence (Tennekes and Lumley, 1972), i.e.

$$2\nu \widetilde{s_{ij} s_{ij}} = 15\nu \left(\widetilde{\frac{\partial u_1'}{\partial x_1}}\right)^2. \tag{6}$$

Equation (6) is substantially accurate because the small-scale eddies contribute most to the dissipation of energy and the small-scale structure of turbulence is very nearly isotopic if the Reynolds number is large. The Reynolds number is

defined as Ul/ν, where U and l are the velocity and length scales of the large eddies. The magnitude of Reynolds number necessary for local isotropy to exist is of the order of 10^5 (Tennekes and Lumley, 1972). Taylor hypothesis is used to determine the turbulent velocity gradient from the single anemometer, i.e.

$$\frac{\partial}{\partial t} = -\tilde{u}_1 \frac{\partial}{\partial x}. \tag{7}$$

Taylor hypothesis states that if $\tilde{u}_1 \gg u_1'$ the temporal fluctuations at a fixed point could be assumed due to the passage of a frozen turbulence pattern past that point, hence the convective derivative could be replaced by the local time derivative. In breaking waves, the turbulent velocities created by the large-scale motions are so large that this condition is not satisified. However, the energy of the small eddies is very much smaller than that of the large eddies, and most of the energy dissipation is associated with small eddies in the inertial and viscous subranges which have large strain rates. Additionally, the small eddies are convected by the large-scale turbulence as well as the organized wave-induced flow. Hence, it may be necessary to separate the small-scale turbulence from the large-scale motion when applied the Taylor hypothesis. In this analysis, turbulent fluctuations contributing to the dissipation of energy are extracted from the turbulent velocity fluctuations u_1' by numerically filtering away frequencies below the inertial subrange, while the advective velocity carrying the small-scale turbulence is obtained from the measured velocity signal u_1 by filtering away frequencies in the inertial and viscous subranges. It is realized that this is an approximation and the results obtained using it must be interpreted with caution; this will be discussed more fully later.

One further approximation, unrelated to the Taylor hypothesis, is used to obtain the energy flux gradients in x. We assume that the wave is of permanent

form such that we can use the transformation

$$\frac{\partial \tilde{u}_j k}{\partial x_j} \approx -\frac{1}{C}\frac{\partial \tilde{u}_j k}{\partial t}, \tag{8}$$

$$\frac{\partial \widetilde{u_j' k'}}{\partial x_j} \approx -\frac{1}{C}\frac{\partial \widetilde{u_j' k'}}{\partial t} \tag{9}$$

where $C = \sqrt{g(H+h)}$ is the wave celerity of finite amplitude long waves. This assumption is good in the inner surf zone where the shape of the broken wave is almost constant, so that the time scale of change in the wave form is much longer than the sampling time interval of 0.01 s. This approximation is not so good in the outer, transition zone where the broken wave is rapidly evolving. It is noted that the propagation speed C was crudely estimated from the time it took for the breaker to travel from one wave gage location to the next wave gage location and it was found that finite amplitude wave theory predicted the wave celerity much better than linear theory for this wave condition.

4. Results and discussions

4.1. Turbulence transport

Experimental results are presented in Fig. 2 through Fig. 6 for different stations in the surf zone. In each figure, the temporal variations of surface elevation and velocity measurements over one wave period are plotted for four different probe depths. The graph line symbols for different probe depths are consistent from top to bottom: solid (—), dash (– – –), dashdot (– · – · –) and dot (· · · · ·).

Figs. 2a–2c show the phase-averaged water surface elevations, horizontal velocities and vertical velocities at breaking ($(x - x_b)/h_b = 0.0$, $h/h_b = 1.0$). Local wave height H is 19.1 cm, wave set-up $\overline{\zeta}$ is -0.25 cm, and mean water

depth h is 15.4 cm. The wave height to water depth ratio H/h is 1.24, which is considerably larger than the value of 0.78 for spilling breakers. This difference is dynamically significant because similar trend is observed throughout the surf zone. It will be shown that the ratio H/h relates to the dynamics of surf-zone turbulence in important ways, and it is a measurable quantity which can be used to distinguish different types of breakers.

Fig. 2b shows that the phase-averaged horizontal velocities are nearly uniform over the water depth, which is to be expected of waves with small water depth to wavelength ratios. Horizontal velocities are approximately $0.35C$ under the crest and $-0.1C$ under the trough. The time-averaged horizontal velocity is seawards; it is about $-0.02C$ at the trough level and the magnitude of the undertow decreases downward. The vertical velocity is large under the steep front of the shoaling wave (Fig. 2c). The maximum upward velocity beneath the wave front is close to $0.2C$ and the maximum downward velocity under the back face of the wave is about $-0.05C$ at the trough level. The time-averaged vertical velocities are downwards, and average about $-0.001C$ in the region between the trough level and the bottom boundary layer. The fluid motion under the wave is not turbulent.

The jet from the overturning wave front plunges into the front face of the original wave. The plunging point is located slightly seaward of the next measuring point ($(x - x_b)/h_b = 3.571$, $h/h_b = 0.929$). At $x = (x - x_b)/h_b = 3.571$, the wave height is 15.1 cm, wave set-up is 0.1 cm, mean water depth is 14.3 cm, and wave height to water depth ratio is 1.06. The falling jet forms a splash when it touches the water, the impact of the jet also pushes up a wedge of water to create a new wave. Both the new wave and the original wave are clearly seen in Figs. 3a–3c. In this initial stage the air tube formed by the closing of the jet on

the water surface is still visible and the jet is plunging into the water. It can be deduced from Figs. 3b and 3c that the impinging jet is deflected downward and backward. It is noted that the instantaneous velocities in the jet could be much larger than the phase-averaged velocities.

The phase-averaged turbulent kinetic energy and energy flux are presented in Figs. 3d–3f. Because the transverse velocity component was not measured, the turbulent kinetic energy is estimated as $k = (1.33/2)\left(\widetilde{u'^2} + \widetilde{w'^2}\right)$ after Stive and Wind (1982), and Svendsen (1987). Comparing Fig. 3d with Figs. 3b and 3c, it is seen that turbulent energy is highest in the jet and turbulent intensity declines immediately after passage of the jet. Turbulent energy also decreases rapidly downward, and it was found that turbulence production below trough level is very small compared to the local time rate of change of turbulent kinetic energy (this will be discussed). The latter suggests that turbulence transport dominates turbulence production below trough level. It is seen that horizontal advection carries turbulent energy forward, except in the jet where turbulent energy are transported backward (Fig. 3e), while vertical advection carries turbulent kinetic energy upward (Fig. 3f) in spite of the downward momentum of the jet; the latter is due to the strong upward flow underneath the wave front. The above results indicate that turbulence is impulsively generated when the plunging jet hits the water, and turbulence under the breaker is spread by large-scale eddy motions.

The momentum and weight of the overturning jet enables it to penetrate the water surface. As the air entrapped by the impinging jet mixes with the water, a region of high vorticity (plunger vortex) and concentration of air bubbles develops. The bubble mass in the plunger vortex rises gradually while translates horizontally at velocities below the wave celerity, so that it appears to move rearward relative to the propagating wave. The wedge of water pushed up by

the plunging jet increases to a height greater than the original wave, and forms another jet which strikes the water ahead of it at a second plunging point. The jet-splash cycles continue at diminishing scale as the wave develops into a turbulent bore, but they are still indentifiable at $(x - x_b)/h_b = 9.740$ ($h/h_b = 0.773$). It is observed that the turbulent bore in the inner surf zone is very intense; the bore front is always tumbling over, and air bubbles carried by large eddies reach the bottom soon after the wave front passes. Since turbulent motion transports fluid particles much more readily than air bubbles it is apparent that vertical mixing of momentum and energy is very strong.

Figs. 4a–4c show the phase-averaged water surface elevations, horizontal velocities and vertical velocities at $(x - x_b)/h_b = 6.494$, $h/h_b = 0.857$. This station is located between the first and the second plunging points. Local wave height is 14.4 cm, wave set-up is 0.27 cm, mean water depth is 13.1 cm, and wave height to water depth ratio is 1.10. It is seen that the phase-averaged velocities have a secondary crest behind the wave front which is not apparent in the surface wave profiles. This is probably because the capacitance wave gage measures the elevation of the aerated water, which includes the surface roller, whereas the LDA only measures the fluid motion due to the wave (the "green water"). The secondary crest is a reminiscence of the original wave; visual observations reveal that the water pushed up by the plunging jet forms a new wave, while the original wave diminishes in the breaking process.

It can be deduced from Fig. 4b that there is a net seaward current (the undertow) under the breaker; the time-mean horizontal velocity is negative. The magnitude of the undertow current is about $0.05C$ in the region between trough level and bottom boundary layer. The time-mean vertical velocity is upwards,

its magnitude is approximately $0.01C$ at trough level and decreasing downward. The phase-averaged turbulent kinetic energy and energy flux are presented in Figs. 4d–4h. Turbulence intensity varies greatly over a wave cycle; it is highest under the wave front and decays rapidly after the wave crest passes. This is indicative of a turbulence decay time that is small compared to the wave period. In the outer surf zone, the jet-splash sequence creates strong vortex motions, and turbulence intensity in the water column increases rapidly with wave propagation distance as the ordered vortex motions degenerate into small-scale motions with increasing disorder. Turbulent energy also decreases downward as shown in Fig. 4d, indicating that turbulent energy is dissipated while convecting downward. The transport of turbulent energy shows that horizontal advection carries turbulent energy shoreward (Fig. 4e), while vertical advection carries turbulent kinetic energy upward under the wave front and downward in the jet (Fig. 4f). Transport of turbulent energy by turbulent velocity fluctuations is given by $\widetilde{u'k'}$ in the horizontal direction and $\widetilde{w'k'}$ in the vertical direction, where $k' = \frac{1}{2}(u'^2 + v'^2 + w'^2)$ is the instantaneous value of turbulent kinetic energy. Unfortunately, we could only measure the components $\frac{1}{2}\widetilde{u'^3}$ and $\frac{1}{2}\widetilde{w'^3}$. It is interesting to see that $\frac{1}{2}\widetilde{w'^3}$ is negative (Fig. 4h), and presumably $\frac{1}{2}\widetilde{u'^2w'}$ and $\frac{1}{2}\widetilde{v'^2w'}$ are also negative, which would mean that large eddies are spreading turbulence downward. Svendsen (1987) conjectured that turbulence under a breaker is spread by convection. This statement now receives some support from Fig. 4h. However, it is necessary to measure all the triple velocity correlation and pressure-velocity correlation terms in order to provide definite proof.

Phase-averaged water surface elevations, horizontal velocities and vertical velocities at $(x - x_b)/h_b = 9.740$, $h/h_b = 0.773$ are presented in Figs. 5a–5c. Local wave height is 11.2 cm, wave setup is 0.53 cm, mean water depth is 11.9 cm,

and wave height to wave depth ratio is 0.94. The magnitude of the undertow is virtually constant below trough level and above bottom boundary layer; it is approximately $0.05C$. The time-averaged vertical velocities are small; it is about $0.005C$ at the trough level and the vertical velocity decreases downward. Comparing Fig. 5c to Fig. 4c, the jet-splash cycle has diminished in scale, but the downward flow due to an impinging jet is still identifiable. The upward flow underneath the wave front is a prominent feature of the broken wave; vertical velocity is close to $0.2C$ at trough level. Phase-averaged turbulent kinetic energy and energy flux are presented in Figs. 5d–5h. Comparing with Figs. 4d-4h, turbulent kinetic energy and energy flux have increased, whereas variations of turbulent energy in the vertical direction have decreased. Since turbulence intensity is highest underneath the wave front and decays rapidly after the wave crest passes, turbulence transport by organized wave-induced flow is landwards. It is apparent from Fig 5e that the horizontal gradients of $\tilde{u}k$ are so large that horizontal advection must play a major role in the distribution of turbulence. Similar conclusions can be drawn about vertical advection (Fig. 5f). In Fig. 5g, the sign of $\frac{1}{2}\widetilde{u'^3}$ is positive, and since this is the largest term in $\widetilde{u'k'}$ it is reasonable to expect that transport of turbulent kinetic energy by turbulent velocity fluctuations is landwards. If the pressure-velocity correlation behaves in the same manner, the turbulent kinetic energy profiles (Fig. 5d) indicate that a counter-gradient transport of turbulent energy has occurred. This could be created by energy transport by large-scale turbulence because the turbulent velocities of the large eddies are well correlated. The above results suggest that such diffusion may not be modeled by the gradient transport model, i.e., Eq. 5. This finding is dynamically significant because Figs. 5e and 5g shows that $\frac{1}{2}\widetilde{u'^3}$ is almost as large as $\tilde{u}k$.

Figs. 6a–6c plot the phase-averaged water surface elevations, horizontal velocities and vertical velocities at $(x - x_b)/h_b = 16.883$, $h/h_b = 0.584$. Local wave height is 7.21 cm, wave set-up is 1.1 cm, and mean water depth is 9.0 cm. The ratio H/h reaches a constant value of 0.8 in the inner surf zone, which is considerably larger than the value of 0.5 for spilling breakers (Svendsen et al. 1978). It is seen that the jet-splash cycles have ceased (Fig. 6c). The velocities of the undertow in the region between trough level and bottom boundary layer are nearly uniform and average $-0.06C$. The time-averaged vertical velocity is about $0.01C$ at trough level and it decreases downward. The phase-averaged turbulent kinetic energy and energy flux are presented in Figs. 6d–6h. It is seen in Fig. 6d that the turbulence levels are very high, and the vertical gradients of turbulent kinetic energy are very small except underneath the wave front. This indicates that turbulent mixing is strong. Figs. 6e and 6g show that horizontal transport of turbulent kinetic energy is landwards; it is dominated by the organized wave-induced flow, and the convection due to the large-scale motions. This is different from spilling breakers where the horizontal transport of turbulence is seawards and dominated by the undertow (see, Ting and Kirby 1994). The behaviour of $\frac{1}{2}\widetilde{w'^3}$ in the inner surf zone is also different from that in the outer surf zone. Comparing Fig. 6h to Fig. 4h, the correlation between w'^2 and w' has become less distinct. This again indicates that the established turbulent flow has thoroughly mixed the water together, and turbulence is convected by large eddies in all directions.

The present experiments differ from those of previous studies (e.g. Stive 1980, Okayasu et al. 1986) in respect of the wave breaking condition. For example, in both afore-mentioned studies plunging breakers have been used and water particle velocities were measured at various locations in the surf zone.

Stive (1980) used a plane beach of slope $m = 0.025$, and the value of H_0/L_0 was 0.01 (test 2). This yields a surf similarity parameter $\xi_0 = m/(H_0/L_0)^{\frac{1}{2}}$ of 0.25. The measurements of Okayasu et al. (1986) were made on a plane beach of slope $m = 0.05$ and the value of H_0/L_0 was 0.0226 (case 2) thus the value of ξ_0 was 0.33. The value of ξ_0 in this present study is 0.60 which is much larger than those used in previous studies. Also, the value of H/h in the inner surf zone is 0.8 compared to 0.54 in Stive (1980). In this respect all the detailed velocity measurements published to date have been conducted for much smaller value of ξ_0, while the wave used in this study falls strongly in the plunging regime.

Variations of H/h in the surf zone with H_0/L_0 have been studied by Svendsen et al. (1978). They used a plane slope of 1 on 34 and deep-water wave steepness H_0/L_0 between 0.0088 and 0.034 (ξ_0 between 0.16 and 0.31). They found that H/h decreases slowly landward, and remains an approximate fixed proportion of the mean water depth in the inner surf zone. Additionally, their data indicate that H/h increases with ξ_0 (the value of H/h varied from 0.4 to 0.6 in the inner surf zone). These results show that wave characteristics in the inner surf zone are different for different deep-water wave conditions although they may be visually similar. Since the large-scale turbulence is created by wave breaking and the large-scale turbulence contributes most to the balance of energy and momentum this suggests that the dynamics of surf-zone turbulence should have certain unique characteristics that are assoicated with a particular wave condition. A comparison of the spatial variations of undertow and time-mean turbulence intensity in spilling and plunging breakers was made in Ting and Kirby (1994). They found that the correlation between mean flow and turbulent kinetic energy is landwards in a plunging breaker and seawards in a spilling breaker. However, they did not study the details of turbulence dynamics

in the spilling and plunging breakers.

An analysis of a number of data sets (e.g. Stive 1980, Hattori and Aono 1985) has been made by Svendsen (1987) concerning turbulence below trough level. Based on certain approximate analytical approaches and experimental measurements, Svendsen (1987) concluded that the temporal variation over a wave period of the turbulent kinetic energy at a fixed point is small, and that the variation over depth of the time mean value of the turbulent kinetic energy is also small. The latter suggests that vertical mixing is strong, which is indicative of the presence of large-scale turbulence structures. Svendsen (1987) also found that only a small portion of the energy loss in a breaker is dissipated below trough level. This dissipation rate is slow, and thus the turbulence level at any given time is the result of many preceding breakers.

The measurements presented in this paper indicate that at large value of ξ_0 wave breaking is so intense that the turbulence levels are much higher. A comparison with the time-mean turbulent kinetic energy, $\overline{k}$, from Stive (1980) for the plunging breaker case was made in Ting and Kirby (1994). It was found that turbulence intensity is much higher in this study compared to Stive (1980). In both cases turbulence levels decrease with distance from the surface but the vertical variations of $(\overline{k}/gh)^{\frac{1}{2}}$ are small. However, turbulence dissipates almost completely over one wave cycle in this study, whereas the dissipation rate was somewhat slower in Stive's experiment. The observed phenomena may be related to the particular wave conditions used in these studies.

The analysis of surf-zone turbulence makes it essential to discuss turbulence length scale and velocity scale. Surf-zone turbulence originates from instabilities of surface waves. Therefore, an important source of energy for the turbulence

is the available kinetic and potential energy released by wave breaking. This suggests that the amount of kinetic energy per unit mass in the large-scale turbulence should increase with the wave height, and a suitable velocity scale for the large-scale turbulence might be the wave celerity based on finite amplitude long waves, i.e., $U = c_1\sqrt{g(H+h)}$. Additionally, the local wave height also imposes a length scale. This is because the large eddies are created by the surface roller therefore the length scale of the large eddies should also depend on the wave height, i.e., $l = c_2 H$. It is expected that the values of the unknown coefficients c_1 and c_2 will depend on ξ_0. If ξ_0 is small the wave is a spilling breaker so turbulence is confined to a region near the crest of the wave. On the other hand, if ξ_0 is large the wave falls strongly in the plunging regime and the whole face of the wave is turbulent. The transition from one breaker type to another is gradual so it is necessary to study waves at the "spilling" end and the "plunging" end of the series in order to distinguish the effect of wave breaking on the flow field.

The local water depth h and the wavelength L provide other length scales which have much influence on the turbulence dynamics. To illustrate what we mean it is useful to compare the rate of vertical mixing with the dissipation rate. We consider an idealized situation in which the production of turbulent energy in the surface roller is modeled by a point source in a two-dimensional flow. We assume that the point source (surface roller) is located at the mean water level and travels at the wave celerity C. From Fig. 6b, the horizontal velocities of the mean flow under the wave crest is about $0.2C$ in the region below trough level and above bottom boundary layer. Hence, turbulent energy created by the surface roller is advected behind the wave front while spreading downward. Neglecting vertical advection, horizontal diffusion, energy dissipation, and production below

trough level, the transport equation for k in a coordinate system that moves with the wave becomes

$$\frac{\partial k}{\partial t} + u\frac{\partial k}{\partial x'} = D\frac{\partial^2 k}{\partial z^2} \tag{10}$$

where $x' = x - Ct$, $u = -0.8C$ is the velocity of the fluid relative to the wave front, and $D = l\sqrt{k}$ is the turbulent diffusion coefficient which is assumed constant (this is a legitimate assumption for $t \ll T$). The boundary conditions of Eq. 10 are the conditions of no transport through the surface and the bottom, i.e., $\partial k/\partial z = 0$ at $z = \overline{\zeta}$ and $z = -d$. This problem is equivalent to transverse mixing of a pollutant discharge at the bank of a river. The time it takes for k to reach within 5% of its mean value everywhere on the vertical section is (see, Fischer et al. 1979)

$$t = 0.4\frac{h^2}{D}. \tag{11}$$

As discussed earlier, the length scale of the large eddies created by the surface roller should be proportional to the local wave height so we assume that $l = H$. Based on Fig. 6d, we use $\sqrt{k} = 0.2C$. After substitution, Equation (11) becomes

$$\frac{t}{T} = \frac{2(h/L)}{(H/h)} \tag{12}$$

where $L = CT$. The dependence of t/T on the wave height parameter, H/h, and the wavelength parameter, h/L, is not surprising. In effect, we are merely saying that the dominant turbulence is associated with large eddies created by the surface roller, therefore the dynamics of turbulence must be related to the wave characteristics.

Taking $H/h = 0.8$ and $h/L = 0.014$, we find that $t/T = 0.035$. This analysis is somewhat simplistic. In particular, the length scale may be too large. Nevertheless, it illustrates that the time scale of mixing is very short under the plunging breaker. The short mixing time is due to large value of

H/h and small value of h/L. Hence, turbulence created in the surface roller is spread almost instantly throughout the water column by convection of large eddies. This is consistent with the experimental observation that the temporal variation of turbulent kinetic energy does not vary significantly with distance from the surface (see, Fig. 6d).

The dissipation rate ϵ is modeled by the classical expression

$$\epsilon = -\frac{C_D}{l} k^{\frac{3}{2}} \tag{13}$$

where $C_D \approx 0.09$ is an empirical constant (Launder and Spalding, 1972). We consider the idealized situation that at $t = 0$ the turbulent kinetic energy is raised to k_0 in the surface roller, from which it decays over the next wave period. The turbulent kinetic energy at time t is (see, Svensden 1987)

$$\frac{k}{k_0} = \frac{1}{(At+1)^2} \tag{14}$$

where $A = C_D k_0^{\frac{1}{2}}/2l$. We could not measure turbulent energy in the surface roller but the turbulence level there is expected to be quite high. From analysis of measurements of frequency of eddy formation we estimated that $\sqrt{k_0} \sim 0.4C$ (this will be discussed) and again we use $l = H$, which yield

$$\frac{k}{k_0} = \left[\frac{0.2C_D(t/T)}{(H/L)} + 1\right]^{-2}. \tag{15}$$

With $H/L = 0.014$, Eq. 15 gives $k/k_0 = 0.19$ at $t/T = 1.0$. Thus most of the turbulent energy is dissipated during one wave cycle. However, the rate of dissipation is much slower than the rate at which turbulent energy is spread downward.

It is apparent from the above analysis that the dynamics of surf-zone turbulence depends on a particular wave condition. The turbulence transport processes in the inner surf zone are not similar for different deep-water wave conditions. The rates of mixing and dissipation are much higher in a plunging

breaker. Because of this, turbulence intensity varies greatly over a wave period. Turbulence level is highest under the wave crest, and declines rapidly after the wave crest passes. The ocurrence of high turbulence intensities with high onshore water particle velocities under the wave crest means that turbulent energy is transported landward (Fig. 6e). In contrast, under a spilling breaker the rates of mixing and dissipation are much lower. The temporal variation of turbulent energy is small therefore turbulence transport is dominated by the undertow current and it is seawards (see, Ting and Kirby 1994). Considering the common assumption of turbulent energy stirring up sediment and making it available for transport by the mean flow, it is natural to expect that the unique characteristics of turbulent flows in spilling and plunging breakers could produce biasing of sediment transport directions. This is consistent with field and laboratory observations that steep waves tend to result in seaward sediment transport and beach erosion, whereas milder and longer waves move sediment onshore and build up beaches. It is conjectured that sediment transport and beach erosion/accretion are tied in a direct way to the dynamics of turbulence in the surf zone. Because of this, it is important to model the spatial and temporal variations of turbulent kinetic energy and its relation to the mean flow in order to correctly predict rates and direction of sediment transport. The interested reader is referred to Ting and Kirby (1994) for a detailed discussion. Since turbulent length scale and velocity scale may be expected to depend on the deep-water wave conditions as well as the beach slope they cannot be specified empirically. The length scale and velocity scale must be determined either on the basis of experimental measurements and/or turbulence modeling (e.g. the k-ϵ model).

4.2. Further analyses

The dynamics of surf-zone turbulence can be elucidated further based on the transport equation for turbulent kinetic energy. Some typical results are presented in Fig. 7 through Fig. 10. In these figures, gradients of turbulent kinetic energy and energy flux are calculated using central finite difference method, and a low-pass filter has been used to filter away any frequencies above 10 Hz since the rates of change of phase-averaged quantities are related to the time scales of large-scale motions. In Fig. 7a the local time rate of change of turbulent kinetic energy, $\partial k/\partial t$, is compared to the advective transport in the horizontal direction, $-\partial \tilde{u}k/\partial x$. These measurements were taken at $(z-\zeta)/h = -0.51$; trough level is located at approximately $(z-\zeta)/h = -0.4$. It is seen that $\partial k/\partial t$ varies periodically behind the wave front. We suspect that this is due to advection of large eddies past the probe. Nadaoka (1986) has measured water particle velocities under a spilling breaker. From flow visualization and velocity measurements, he concluded that there exists a characteristic large-scale eddy structure under the spilling breaker consisting of two-dimensional eddies around the wave crest and three-dimensional vortices extending obliquely downward; the large eddies are identifiable for only a short time, and similar, although not identical structures occur repeatedly in successive breakers. Using laser-induced fluorescent technique, Yeh and Mok (1990) studied turbulent bores created in the dam-break problem. They observed sporadic, three-dimensional turbulence patches in the turbulent flow region behind the bore front and conjectured that these turbulence patches are created by intermittent advection of the recirculating flow of the surface roller. From Fig. 7a, the frequency of oscillation is about 7 Hz. Assuming one large eddy is formed within one "turnover time" of the recirculating flow in the surface roller, the frequency of eddy formation is l/U,

where l and U represent the length scale and velocity scale of the recirculating flow in the surface roller. If we take $U = 0.4C$ and $l = H$, which are quite reasonable values, the predicted frequency would be 7 Hz in agreement with the experimental data. Fig. 7a indicates that the frequency of turbulence patch generation is high in the plunging breaker. On the other hand, the large eddies have short decay time and they break down rapidly into small-scale turbulence so only a few turbulence patches can be seen behind the wave front.

Fig. 7a shows that the temporal variation of turbulent kinetic energy at a fixed point is directly related to the gradient transport of turbulent energy by mean flow in the horizontal direction. This can be expected because the rates of mixing and energy dissipation are both high in the plunging breaker. The generated turbulence immediately saturates the entire flow depth and is carried past the probe by the mean flow therefore the time rate of change of k is mostly produced by turbulence transport in the horizontal direction. The dissipation rate is also high in the plunging breaker so turbulence dies out between bores. When the next breaker comes, new bursts of turbulence are generated and advected past the probe. We have done a similar analysis for a spilling breaker and find that $\partial k/\partial t$ does not correlate well with $-\partial \tilde{u} k/\partial x$ in the spilling breaker (not shown), which suggests that the time rate of change of turbulent energy under a spilling breaker is not dominated by mean flow advection. We found that the temporal variation over a wave period of the turbulent kinetic energy at a fixed point is small under the spilling breaker (see, Ting and Kirby 1994), so that gradient transport of k in the horizontal direction is small. In addition, vertical mixing in the spilling breaker is much slower. Hence, temporal variation of k under the spilling breaker is more dominated by downward spreading of surface-generated turbulence into the fluid domain than by horizontal advection

of turbulent energy past the probe. Fig. 7a indicates that horizontal advection by organized wave-inducted flow plays a major role in the distribution of turbulence under the plunging breaker. Hence, its effect must be considered in turbulence modeling to correctly predict the temporal and spatial variations of turbulent kinetic energy.

The advective transport in the vertical direction $-\partial\tilde{w}k/\partial z$ is presented in Fig. 7b. This term is also important; it is seen that $\partial k/\partial t$ and $-\partial\tilde{w}k/\partial z$ are of the same order of magnitude. Vertical advection removes turbulent energy locally, and carries it toward the free surface. This conclusion can be reached by inspection of Fig. 6f, which clearly shows that vertical gradients of $\tilde{w}k$ are positive. Since this does not have a corresponding effect on the temporal variation of k, we conjecture that the energy removed is replaced by production and/or diffusion.

It would be important to examine the diffusive transport due to velocity and pressure fluctuations. Available measurements indicate that turbulent diffusion deposits kinetic energy from the surface roller, but the results are inconclusive because we did not measure all the diffusion terms. The temporal variation of $-\frac{1}{2}\partial\widetilde{u'^3}/\partial x$ is presented in Fig. 7c. This term is a major part of $-\partial\widetilde{u'k'}/\partial x$ which represents the gradient transport of k' by the horizontal component of turbulent velocity fluctuations. Hence, we may expect that $-\partial\widetilde{u'k'}/\partial x$ behaves in a similar manner. It is seen that $\partial k/\partial t$ and $-\frac{1}{2}\partial\widetilde{u'^3}/\partial x$ are well correlated. This again indicates that turbulent energy is convected past the probe by large eddies under the plunging breaker. The temporal variation of $-\frac{1}{2}\partial\widetilde{w'^3}/\partial z$ is plotted in Fig. 7d. This term is only part of $-\partial\widetilde{w'k'}/\partial z$, which represents the gradient transport of k' by the vertical component of turbulent velocity fluctuations. It is seen that $-\frac{1}{2}\partial\widetilde{w'^3}/\partial z$ is much smaller, but this does not imply that $-\partial\widetilde{w'k'}/\partial z$ is also

small. Thus, no definite conclusion can be drawn about vertical diffusion.

The results for $(z-\zeta)/h = -0.73$ are presented in Figs. 8a–8d. The local time rate of change of k decreases with distance from the surface but the periodic fluctuations of $\partial k/\partial t$ can still be seen near the bottom, which indicates that large-scale structure is a dominant feature of the turbulence dynamics under the plunging breaker. It is seen that vertical advection and diffusion are important in the bottom region (Figs. 8b and 8d). The latter is to be expected since turbulent kinetic energy is spread downward by diffusion. Similar patterns as those shown in Figs. 7 and 8 are found for other locations in the surf zone.

The major terms of turbulence production are presented in Figs. 9a–9d for $(z-\zeta)/h = -0.51$. We could not measure the Reynolds stress $-\widetilde{u'w'}$. However, in most shear flows the correlation coefficient between u' and w' is about 0.4, and this value varies only little from flow to flow (see, Townsend 1976). This similarity of turbulent motion is related to the straining of large eddies by shearing. It can be shown by order of magnitude analysis that u' and w' has to be well correlated if a balance between production and dissipation, however approximate, is to be obtained (see, Tennekes and Lumley 1972), and indeed, turbulence production and dissipation are of the same order of magnitude in many shear flows. Hence, we may expect that the term $-\widetilde{u'w'}\partial\tilde{u}/\partial z$ is of order $(\widetilde{u'^2}\widetilde{w'^2})^{\frac{1}{2}}\partial\tilde{u}/\partial z$ (Fig. 9a). This term represents the energy removed from the mean flow by the work of Reynolds shear stress against the mean velocity gradient. It accounts for most of the turbulence production below trough level. Fig. 9a indicates that turbulence production is large under the wave front, which is related to the high turbulence intensity and shear rate there (see, Figs. 6b and 6d). In contrast, the term $-\widetilde{u'w'}\partial\tilde{w}/\partial x$, which is of order $(\widetilde{u'^2}\widetilde{w'^2})^{\frac{1}{2}}\partial\tilde{w}/\partial x$, is vanishingly small (Fig. 9b). The production term caused by normal-stress dif-

ference $-(\widetilde{u'^2} - \widetilde{w'^2})\partial\tilde{u}/\partial x$ is also small since it is the difference between $\widetilde{u'^2}$ and $\widetilde{w'^2}$ that determines the contribution to turbulence production (Figs. 9c and 9d). The results for $(z-\zeta)/h = -0.71$ are plotted in Figs. 10a-10d and are similar to Figs 9a-9b. It is seen that turbulence production has decreased in the bottom region. This analysis was repeated for other locations in the surf zone, and it was found that the relative importance of turbulence production below trough level becomes small in the outer surf zone.

Since we did not measure u' and w' simultaneously, the production term $\widetilde{u'w'}\partial\tilde{u}/\partial z$ is assumed equal to $0.4(\widetilde{u'^2}\widetilde{w'^2})^{\frac{1}{2}}\partial\tilde{u}/\partial z$. On the basis of published results in shear flows we expect that the error associated with this estimation will not exceed $\pm 25\%$. The turbulent energy production obtained in this way is averaged over one wave period and plotted in Fig. 11. The results indicate that turbulence production decreases with distance from the surface. At the present time, it is believed that the surface roller is the source of most of the turbulent energy but there are no measurements to confirm this hypothesis. It is not possible to measure energy production in the surface roller due to difficulties with instrumentation in aerated water. Hence, we shall examine the energy production below trough level and compare it to the loss of wave energy in the broken wave.

The equation for energy balance averaged over one wave period is (see, Svendsen 1984)

$$\frac{\partial E_{f,w}}{\partial x} = -D_t \tag{16}$$

where $E_{f,w}$ is the flux of organized wave energy and D_t is the production of turbulent kinetic energy per unit area. Eq. 16 equates the wave energy loss to turbulent energy production, so that we do not have to consider the flux of

turbulent energy. Svendsen (1984) expressed $E_{f,w}$ as

$$E_{f,w} = \rho g c H^2 B \tag{17}$$

where H is the wave height, c is defined as $\sqrt{gh}$ and B is a dimensionless coefficient given by

$$B = \overline{\left(\frac{\zeta}{H}\right)^2} + \frac{1}{2}\frac{A}{H^2}\frac{h}{L}. \tag{18}$$

In Eq. 18, A is the cross-sectional area of the surface roller and $L = cT$ is the local wavelength based on linear theory. For this plunging breaker, the value of $\overline{\left(\frac{\zeta}{H}\right)^2}$ in the inner surf zone is 0.08 but the value of A is not known. Svendsen (1984) used $A = 0.9H^2$ based on the experiments of Duncan (1981). Svendsen (1984) then studied the variation of B with h/h_b for different deep water wave conditions and found that B approaches values around 0.07-0.08 in the inner surf zone. Hence, B may be expected to be ~ 0.1 in this case.

Substituting Eq. 17 into Eq. 16, we obtain

$$\frac{D_t}{\rho h(c^2/T)} = -\frac{5}{2}\left(\frac{H}{h}\right)^2 B\frac{h_x}{h/L} \tag{19}$$

where h_x equals minus the bottom slope. Using $B = 0.1$, $h_x = -1/35$, $h/L = 0.0192$, we get $D_t/\rho h(c^2/T) = 0.238$. Turbulent energy production below trough level is found from experimental measurements as

$$\frac{0.4}{hT}\int_{-d}^{\zeta_{tr}}\int_0^T \frac{(\widetilde{u'^2}\widetilde{w'^2})^{\frac{1}{2}}\partial\tilde{u}/\partial z}{(c^2/T)}dtdz \tag{20}$$

where $z = \zeta_{tr}$ is the trough level. By numerical integration, we find that about 7% of the total turbulent energy is generated below trough level.

In the one-equation model the dissipation rate is usually modeled using Eq. 13, which follows from dimensional analysis. The major weakness of the one-equation model is that the specification of the length scale l is rather arbitrary.

Previously, Deigaard et al. (1985) used $l = 0.07h$, whereas Svendsen (1987) used $l = 0.2h$. Using Eq. 13 and the measured dissipation rate, we find that the length scale is almost constant in the region below trough level and above bottom boundary layer; it is $\sim$ 0.08-0.1h (this will be discussed). With $l = 0.1h$ and k from experiment, the energy dissipation is predicted using Eq. 13. The dissipation rate averaged over one wave period is compared to the production rate in Fig. 11. It is seen that the dissipation rate decreases with distance from the surface but its vertical variation is small. This is due to the quite high turbulence intensities near the bottom. Fig. 11 indicates that energy dissipation is higher than turbulence production below trough level, which is to be expected. It was found that about 16% of the turbulent energy is dissipated below trough level.

The variations of the predicted dissipation rate with time are plotted in Fig. 12 for different vertical locations. Comparing Fig. 12 to Figs. 9 and 10, the rate at which energy is dissipated is much smaller than the time rate of change of k. This is to be expected because the rate of dissipation is governed by the rate of energy transfer from the large eddies to the small-scale turbulence and is proportional to $k^{\frac{3}{2}}/l$, where k and l represent the turbulent kinetic energy and length scale of the large eddies, respectively. On the other hand, the time rate of change of k is mostly produced by turbulence structure blowing past the probe rather than by changes in the turbulence structure itself. Thus, it is not surprising that $\partial k/\partial t$ should be much larger than ϵ.

The measured dissipation rates are also plotted in Fig. 12. As mentioned in § 3, the turbulent fluctuations contributing to energy dissipation are found from u' by numerically filtering away frequencies below the inertial subrange, while the convective velocities are obtained from u by filtering away frequencies

in the inertial and viscous subranges, and in order to satisfy Taylor hypothesis we use only those data where the turbulent velocities are much smaller than the convective velocities ($|u'/u| < 0.1$ in this case). Here, u' and u refer to the filtered velocities. Fig. 12 shows that the measured dissipation rates are too low during the crest portion of the wave. A sensitivity analysis was conducted by varying the value of $|u'/u|$ from 0.1 to 1.0. It was found that under the wave crest the dissipation rate increases as $|u'/u|$ increases but under the wave trough energy dissipation is insensitive to changes in $|u'/u|$. Hence, the length scale of turbulence l is estimated from the measured dissipation rates from the trough portion of the wave. We found that the length scale is almost constant and $\sim 0.1h$. With this result the predicted dissipation rates are obtained using Eq. 13 and k from the experiments. This analysis reveals problems associated with the use of Taylor hypothesis in the surf zone. As experimental technqiues improve, energy dissipation under breaking waves will be examined again.

5. Conclusions

The spatial distributions and time histories of two velocity components under a strong plunging breaker were measured using a fiber-optic laser-Doppler anemometer at several locations in the surf zone in the region below trough level and above bottom boundary layer. The turbulence transport and the equation governing the phase-averaged turbulent kinetic energy k were examined based on these velocity measurements. The following main conclusions can be drawn from this investigation:

1. The turbulence structure in a plunging breaker has unique features that can be related to its wave characteristics. The important wave parameters are the wave height to water depth ratio H/h and the water depth to

wavelength ratio h/L. Based on approximate analytical approaches and experimental data we find that the dynamics of surf-zone turbulence depends on the deep-water wave condition and the beach slope. Similarly, the length scale and velocity scale of the large-scale turbulence depend on a particular wave condition. Laboratory measurements indicate that turbulent flows in spilling and plunging breakers are fundamentally different. However, a gradual transition may be expected from one breaker type to another.

2. The temporal variation over a wave period of the turbulent kinetic energy at a fixed point under the plunging breaker is large. Turbulence intensity is highest under the wave front and decreases rapidly after the wave crest passes so turbulence dies out between breakers. Turbulent energy transport by organized wave-induced flow is landwards. If it is assumed that sediment transport is tied in a direct way to turbulence transport, then suspended sediment could be moved onshore under the plunging breaker.

3. The rate of vertical mixing is high in a plunging breaker. This is due to large value of H/h and small value of h/L. Turbulence is spread downward by the large eddies. In the inner surf zone, turbulence created by the surface roller immediately saturates the entire flow depth and advected behind the wave front. Because of this, the time rate of change of turbulent kinetic energy at a fixed point is mostly produced by transport of turbulence structure in the horizontal direction.

4. Experimental measurements indicate that large eddies are generated at regular interval in the surface roller and advected behind the wave front. The frequency of eddy formation can be related to the length scale and velocity scale of the surface roller.

5. It is found that advective and diffusive transport of turbulence are both important in the inner surf zone. The dynamics of surf-zone turbulence is controlled by turbulence transport of large-scale structures. The turbulence generated seaward is transported landward by convection so that the turbulent flow pattern moving landward is strongly dependent on its history. Turbulence production and energy dissipation are not in local equilibrium but are of the same order of magnitude and they amount to only a small fraction of the energy loss in the broken wave.

Acknowledgements

This study was funded by the Office of Naval Research under contract N-00014-90-J1678. F.C.K.T also acknowledges the support of the Texas Higher Education Coordinating Board through Grant 999903-261.

References

Basco, D. R., 1985. A qualitative description of wave breaking. J. Waterw., Port, Coastal Ocean Eng. ASCE, 111: 171–188.

Battjes, J. A., 1988. Surf-zone dynamics. Annu. Rev. Fluid Mech., 20: 257–293.

Deigaard, R., Fredsœ, J. and Hedegaard, I. B., 1985. Suspended sediment in the surf zone. J. Waterw., Port, Coastal Ocean Eng. ASCE, 111: 115–128.

Duncan, J. H., 1981. An experimental investigation of breaking waves produced by a towed hydrofoil. Proc. Roy. Soc. Lond., A 377: 311–348.

Fischer, H. B., List, E. J., Koh, R. C. Y., Imberger, J. and Brooks, N. H., 1979.

Mixing in inland and Coastal Waters. Academic Press, 483pp.

Hattori, M. and Aono, T., 1985. Experimental study on turbulence structures under breaking waves. Coastal Eng. in Japan, 28: 97–116.

Launder, B. E. and Spalding, D. B., 1972. Mathematical models of turbulence. Academic Press.

McLellan, T. N., 1990. Nearshore mound construction using dredged material. J. Coastal Res., 7: 99–107.

McLellan, T. N. and Kraus, N. C., 1991. Design guidance for nearshore berm construction. In: Proc. Coastal Sediments '91, Seattle. ASCE, New York, pp. 2000–2011.

Mizuguchi, M., 1986. Experimental study on kinematics and dynamics of wave breaking. In: Proc. 20th Int. Coastal Eng. Conf., Taipei. ASCE, New York, pp. 589–603.

Nadaoka, K., 1986. A fundamental study on shoaling and velocity field structure of water waves in the nearshore zone. Tech. Report. No. 36, Dept. Civ. Eng., Tokyo Inst. Tech., Japan.

Nakagawa, T., 1983. On characteristics of the water-particle velocity in a plunging breaker. J. Fluid Mech., 126: 251–268.

Okayasu, A., Shibayama, T. and Nimura, N., 1986. Velocity field under plunging waves. In: Proc. 20th Int. Coastal Eng. Conf., Taipei. ASCE, New York, 660–674.

Peregrine, D. H., 1983. Breaking waves on beaches. Annu. Rev. Fluid Mech.,

15: 149–178.

Rodi, W. 1984. Turbulence models and their application in hydraulics - A state of the art review. IAHR, 104pp.

Stive, M. J. F., 1980. Velocity and pressure field of spilling breakers. In: Proc. 17th Int. Coastal Eng. Conf., Sydney. ASCE, New York, 547–566.

Stive, M. J. F. and Wind, H. J., 1982. A study of radiation stress and set-up in the surf zone. Coastal Eng., 6: 1–25.

Svendsen, I. A., 1987. Analysis of surf zone turbulence. J. Geophys. Res., 92(C5): 5115–5124.

Svendsen, I. A., Madsen, P. A. and Buhr Hansen, J., 1978. Wave characteristics in the surf zone. In: Proc. 16th Int. Coastal Eng. Conf., Hamburg. ASCE, New York, 520–539.

Tennekes, H. and Lumley, J. L., 1972. A first course in turbulence. MIT Press, 300pp.

Ting, F. C. K. and Kirby, J. T., 1994. Observation of undertow and turbulence in a laboratory surf zone. Coastal Eng., (in press).

Yeh, H. H. and Mok, K. M., 1990. On turbulence in bores. Physics of Fluids, 2: 821-828.

Table 1

Wave Conditions (the subscripts 0, h and b denote deep water, horizontal section and breaking point)

H_0 (m)	H_h (m)	H_b (m)	T (s)	H_0/L_0	x_b (m)	d_b (m)
0.089	0.128	0.191	5.0	0.0023	7.795	0.156

Locations of measurements and water depths

x (m)	7.295	7.795	8.345	8.795	9.295	9.795	10.395
d (m)	0.169	0.156	0.142	0.128	0.113	0.096	0.079
h (m)	0.166	0.154	0.143	0.132	0.119	0.104	0.090

LIST OF FIGURES

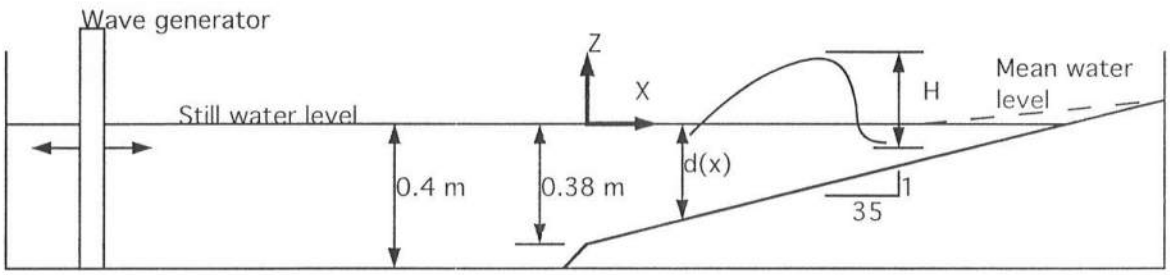
Wave generator
Z
X
H
Mean water level
Still water level
0.4 m
0.38 m
d(x)
1
35

FIGURE 1

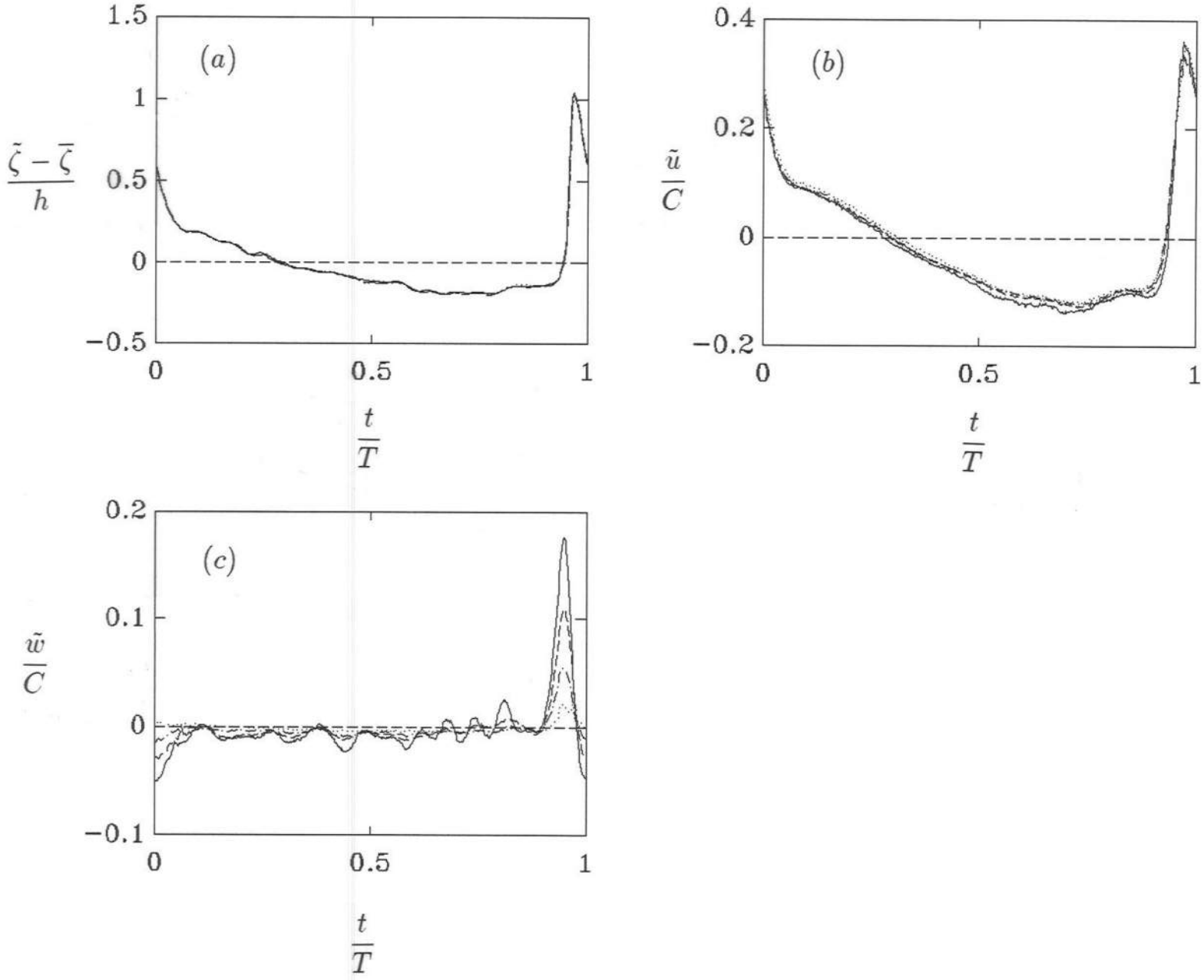
(a)
1.5
1
0.5
0
−0.5
0
0.5
1
$\frac{\tilde{\zeta}-\overline{\zeta}}{h}$
$\frac{t}{T}$
(b)
0.4
0.2
0
−0.2
0
0.5
1
$\frac{\tilde{u}}{C}$
$\frac{t}{T}$
(c)
0.2
0.1
0
−0.1
0
0.5
1
$\frac{\tilde{w}}{C}$
$\frac{t}{T}$

FIGURE 2

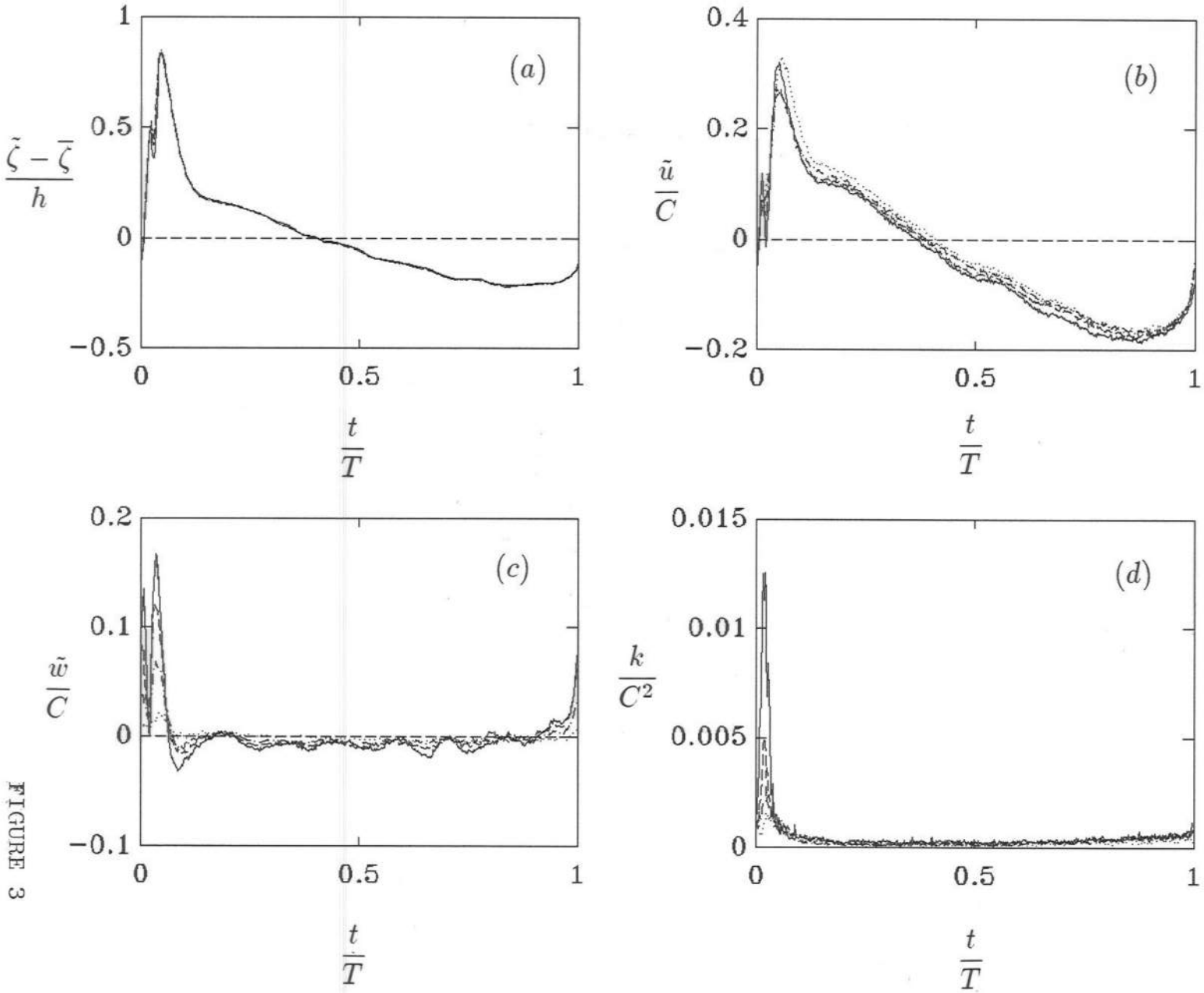
(a)
(b)
(c)
(d)
$\frac{\tilde{\zeta}-\overline{\zeta}}{h}$
$\frac{\tilde{u}}{C}$
$\frac{\tilde{w}}{C}$
$\frac{k}{C^2}$
$\frac{t}{T}$
1
0.5
0
−0.5
0.4
0.2
−0.2
0.1
−0.1
0.015
0.01
0.005

FIGURE 3

FIGURE 3 (continued)

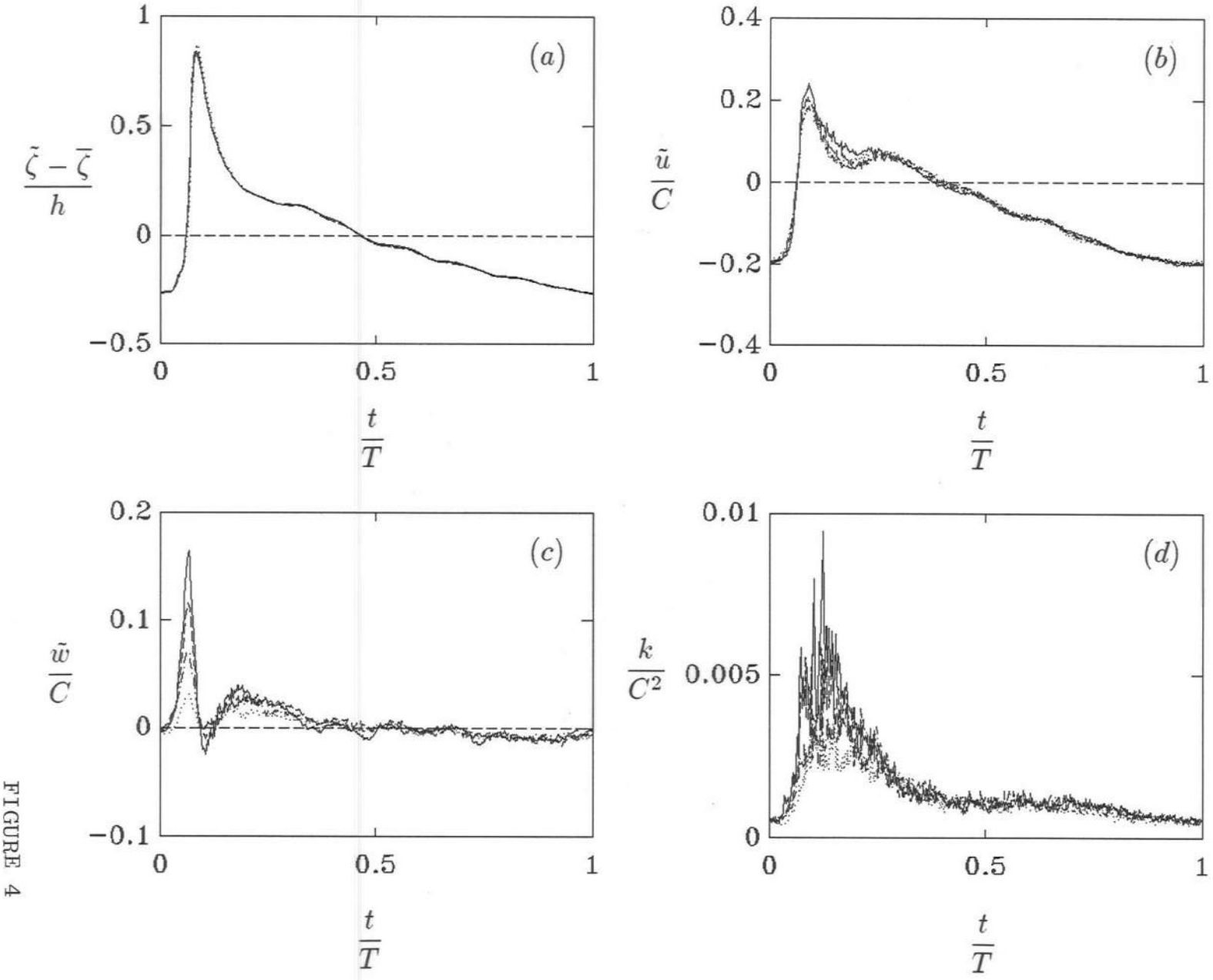
(a)
$\frac{\tilde{\zeta}-\overline{\zeta}}{h}$
1
0.5
0
−0.5
0
0.5
1
$\frac{t}{T}$
(b)
$\frac{\tilde{u}}{C}$
0.4
0.2
0
−0.2
−0.4
0
0.5
1
$\frac{t}{T}$
(c)
$\frac{\tilde{w}}{C}$
0.2
0.1
0
−0.1
0
0.5
1
$\frac{t}{T}$
(d)
$\frac{k}{C^2}$
0.01
0.005
0
0
0.5
1
$\frac{t}{T}$

FIGURE 4

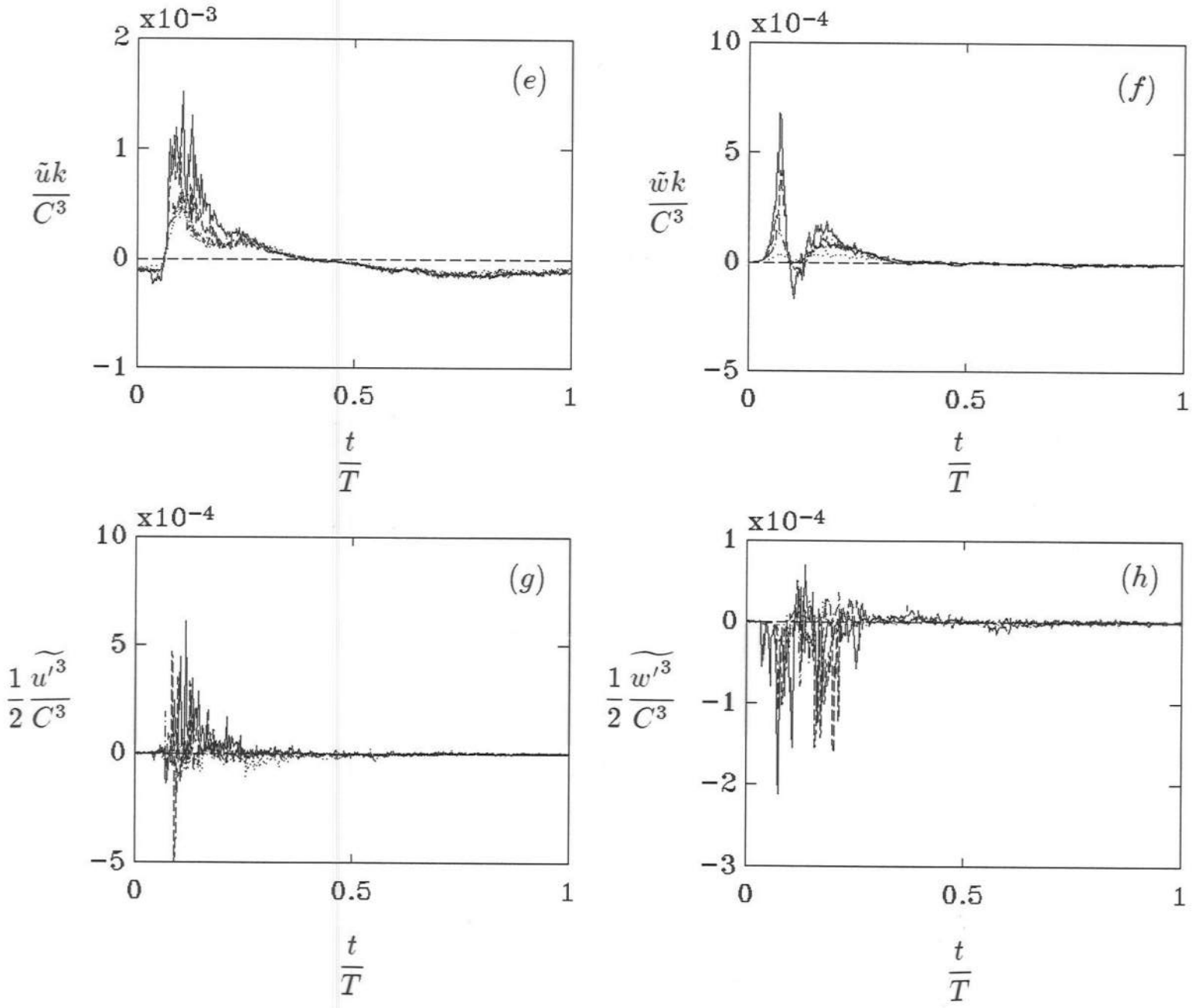

FIGURE 4 (continued)

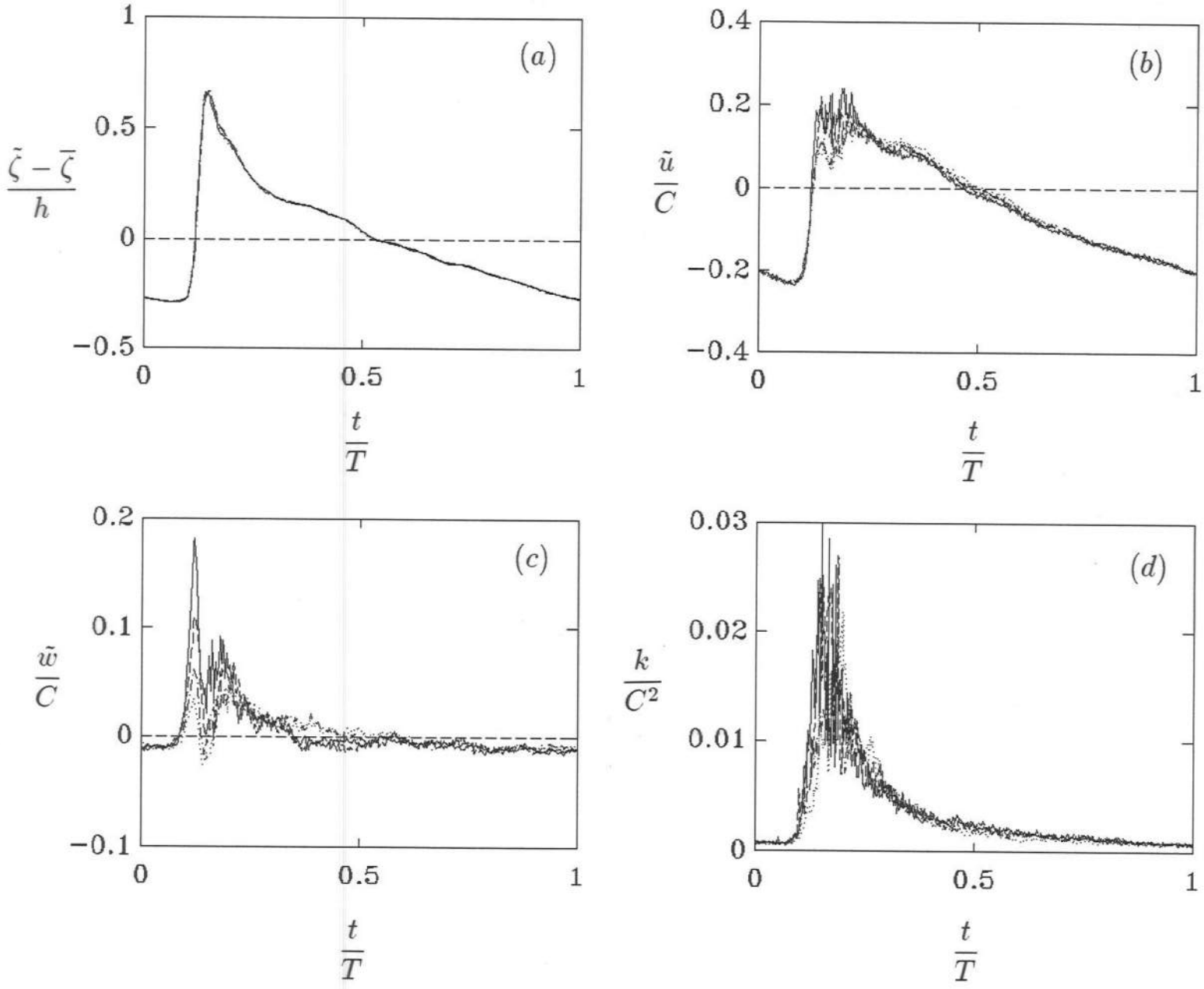
(a)
$\frac{\tilde{\zeta}-\overline{\zeta}}{h}$
1
0.5
0
−0.5
0
0.5
1
$\frac{t}{T}$
(b)
$\frac{\tilde{u}}{C}$
0.4
0.2
0
−0.2
−0.4
0
0.5
1
$\frac{t}{T}$
(c)
$\frac{\tilde{w}}{C}$
0.2
0.1
0
−0.1
0
0.5
1
$\frac{t}{T}$
(d)
$\frac{k}{C^2}$
0.03
0.02
0.01
0
0
0.5
1
$\frac{t}{T}$

FIGURE 5

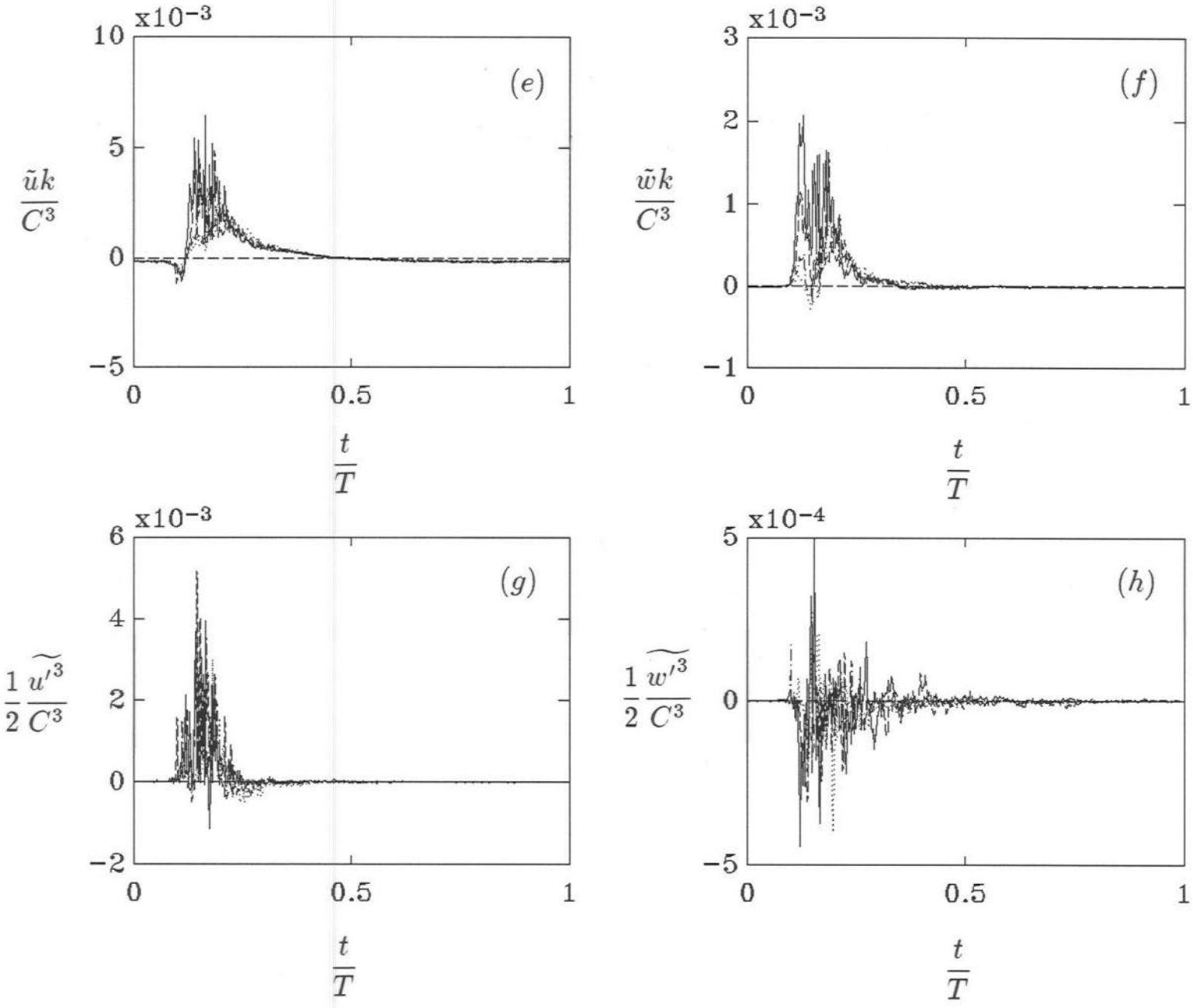

FIGURE 5 (continued)

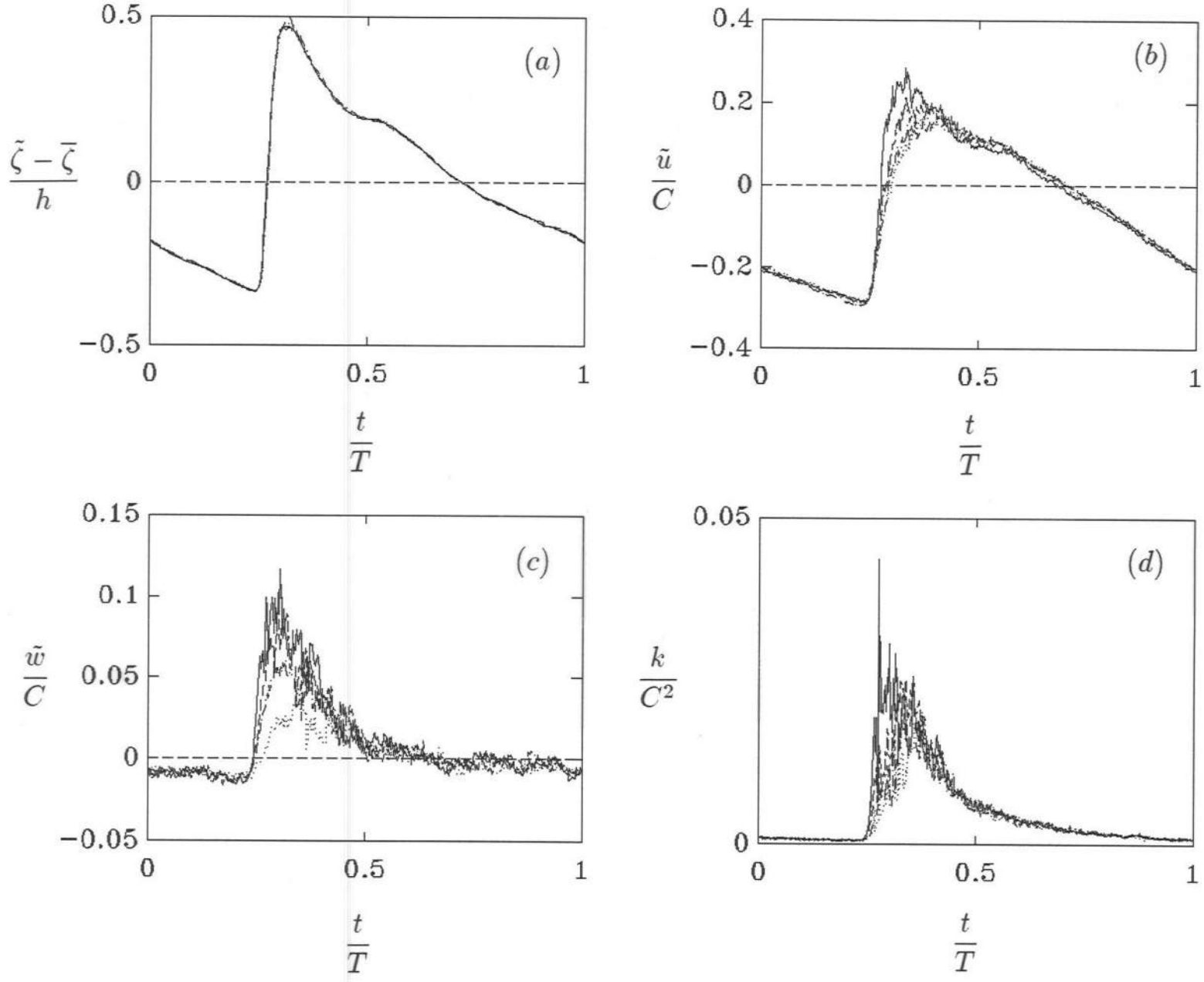
(a)
0.5
0
−0.5
$\frac{\tilde{\zeta}-\overline{\zeta}}{h}$
0
0.5
1
$\frac{t}{T}$
(b)
0.4
0.2
0
−0.2
−0.4
$\frac{\tilde{u}}{C}$
0
0.5
1
$\frac{t}{T}$
(c)
0.15
0.1
0.05
0
−0.05
$\frac{\tilde{w}}{C}$
0
0.5
1
$\frac{t}{T}$
(d)
0.05
0
$\frac{k}{C^2}$
0
0.5
1
$\frac{t}{T}$

FIGURE 6

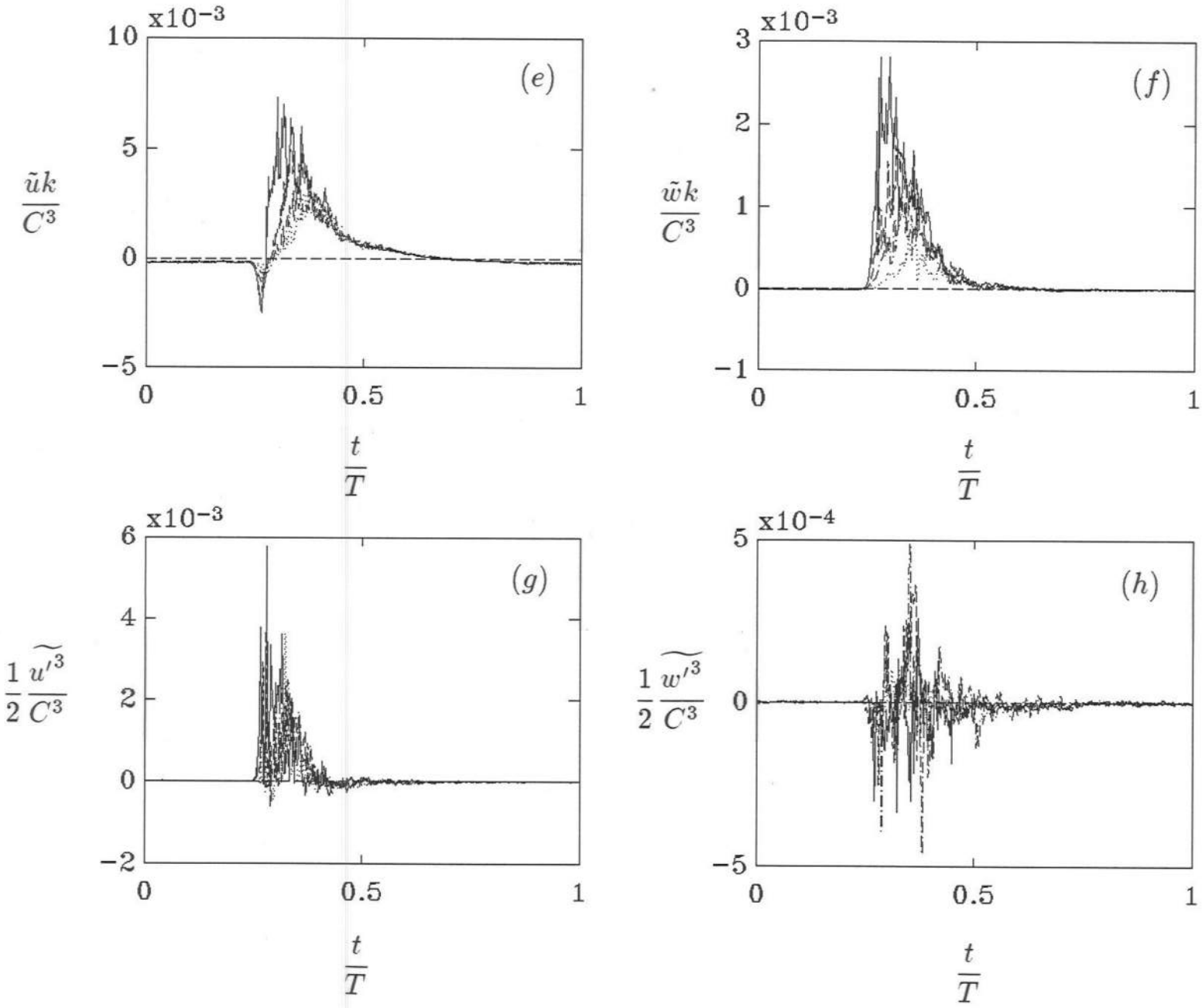

FIGURE 6 (continued)

(a)
(b)
(c)
(d)
$-\frac{\partial \tilde{u}k}{\partial x}/(C^2T^{-1})$
$-\frac{\partial \tilde{u}k}{\partial z}/(C^2T^{-1})$
$-\frac{1}{2}\frac{\partial \widetilde{u'^3}}{\partial x}/(C^2T^{-1})$
$-\frac{1}{2}\frac{\partial \widetilde{w'^3}}{\partial z}/(C^2T^{-1})$
$\frac{t}{T}$
$\frac{t}{T}$
$\frac{t}{T}$
$\frac{t}{T}$
2
1
0
−1
−2
0
0.5
1

FIGURE 7

(a)
$-\frac{\partial \tilde{u}k}{\partial x}/(C^2T^{-1})$
(b)
$-\frac{\partial \tilde{w}k}{\partial z}/(C^2T^{-1})$
(c)
$-\frac{1}{2}\frac{\partial \widetilde{u'^3}}{\partial x}/(C^2T^{-1})$
(d)
$-\frac{1}{2}\frac{\partial \widetilde{w'^3}}{\partial z}/(C^2T^{-1})$
1
0.5
0
−0.5
$\frac{t}{T}$

FIGURE 8

(a)
(b)
(c)
(d)
$(\widetilde{u'^2w'^2})^{\frac{1}{2}}\frac{\partial\tilde{u}}{\partial z}/(C^2T^{-1})$
$(\widetilde{u'^2w'^2})^{\frac{1}{2}}\frac{\partial\tilde{u}}{\partial x}/(C^2T^{-1})$
$-\widetilde{u'^2}\frac{\partial\tilde{u}}{\partial x}/(C^2T^{-1})$
$-\widetilde{w'^2}\frac{\partial\tilde{u}}{\partial z}/(C^2T^{-1})$
$\frac{t}{T}$
$\frac{t}{T}$
$\frac{t}{T}$
$\frac{t}{T}$
2
1
0
−1
−2
0
0.5
1

FIGURE 9

(a)
(b)
(c)
(d)
1
0.5
0
−0.5
0
0.5
1
$\frac{t}{T}$
$(\widetilde{u'^2w'^2})^{\frac{1}{2}}\frac{\partial\tilde{u}}{\partial z}/(C^2T^{-1})$
$(\widetilde{u'^2w'^2})^{\frac{1}{2}}\frac{\partial\tilde{w}}{\partial x}/(C^2T^{-1})$
$-\widetilde{u'^2}\frac{\partial\tilde{u}}{\partial x}/(C^2T^{-1})$
$-\widetilde{w'^2}\frac{\partial\tilde{w}}{\partial z}/(C^2T^{-1})$

FIGURE 10

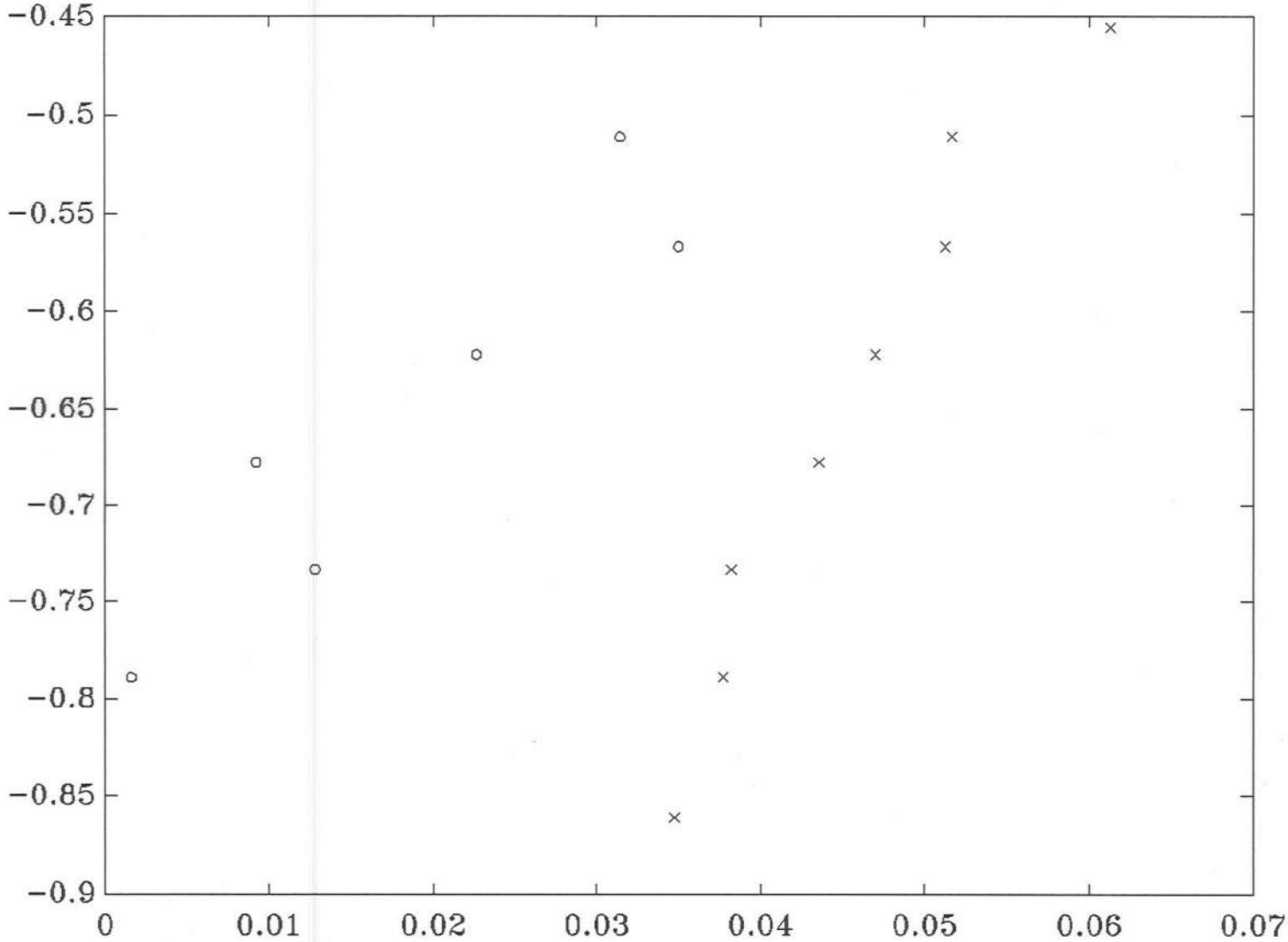

Time-averaged production and dissipation

FIGURE 11

FIGURE 12